

Structural Response of Offshore Monopile Foundations to Ocean Waves

M. Li, H. Song, H. Zhang and H. Guan
Griffith School of Engineering, Griffith University
Gold Coast, QLD, Australia

ABSTRACT

Offshore monopile foundations are one of the most commonly used foundation concepts in offshore renewable energy, especially in areas with relatively shallow water. They are characterised by relatively large geometric dimensions compared with other offshore pile foundations and are distinguished from onshore piles by suffering from harsh ocean environments during their lifetime. One of the most significant aspects is associated with the wave effect on the behaviour of monopile foundations. To date, research has been conducted in the development of numerical models, which are capable of providing sophisticated and flexible representations of the monopile foundations. In this study, a three-dimensional scaled boundary finite element model (SBFEM) is proposed to investigate the structural response of the monopile foundations when exposed to ocean waves. Unlike other numerical techniques, SBFEM provides an analytical solution in the radial direction with numerical approximation along the circumferential and top faces of the monopile foundation, which considerably reduces the computational effort. The SBFEM model is validated by an equivalent finite element model, by which favourable computational efficiency and reliable accuracy are demonstrated. Subsequently, a parametric study is carried out in terms of various wave properties to gain an insight into the monopile behaviour. The purpose of this study is to make recommendations for improving the design of offshore monopile foundations, when wave load is a dominant factor.

KEY WORDS: Offshore monopile foundations; ocean waves; structural behaviour; scaled boundary finite element model; three-dimensional

INTRODUCTION

Offshore wind farms, as a competitive resource of renewable energy, currently are, and potentially will be, gaining even more global popularity, as they provide higher economic returns and are less obstructive than onshore wind farms. Among the foundation concepts, monopile foundations have been receiving significant attention, particularly when the water depth is no more than 50 meters. They are characterised by a large but simple geometric configuration and localised seabed consumption, consequently simplifying the installation

process and minimising environmental disturbance. Furthermore, experience is available from the classic pile foundation topic, which has been studied for decades in both ocean engineering and geotechnical engineering. Monopile foundations, used in offshore renewable energy applications, are often identified by their relatively large diameter, compared with the commonly used pile foundations in other offshore applications; also, they differ from the deep pile foundation in geotechnical engineering since wave loads are considered as one of the key factors in monopile foundation design. Therefore, understanding of the monopile foundation behaviour subjected to wave loads in ocean environment is of great importance.

Progress has been achieved in the past few years regarding the monopile foundation behaviour under the lateral loading associated with winds, waves and the seabed, especially in Northern Europe, where offshore wind farm development was pioneered. Kellezi and Hansen (2003) presented both static and dynamic models of the foundation, however, they only addressed the geotechnical aspect, namely, the monopile-seabed interaction. Zaijier (2006) explored the foundation sensitivity to wave and wind loads by simply using excitation frequencies to represent the wave and wind influence. Achmus et al. (2009) developed a degradation stiffness model to account for the loading effect from the ocean waves. Eicher et al. (2003) studied the stress and deformation of a 1 m radius pile, a general offshore pile, under combined structural and wave loads. To date, there has been a dearth of explicit research in large-diameter monopile foundation behaviour under wave load conditions.

The objective of this study is to investigate the effects of the wave loads on monopile foundations and how the monopile responses to the variation of several key parameters of the wave loads. A three-dimensional numerical model is proposed herein based on SBFEM, which was first conceptualised by Wolf and Song (1996). By combining the advantages of two powerful numerical techniques, namely, the Finite Element Method (FEM) and the Boundary Element Method (BEM), the SBFEM has found its broad applicability in various engineering aspects. Wolf (2002), Doherty and Deeks (2003) and Khani (2007) employed this method to investigate the soil-structure interaction in geotechnical engineering, in which the superior performance of SBFEM over FEM and BEM in dealing with the unbounded nature of soil domain has been fully demonstrated. Yang (2006) and Yang and Deeks (2007) developed an automatic crack growth model using SBFEM, further validating its capability in dealing

with the stress intensification at the sharp crack tips. Deeks and Cheng (2003), Li (2007), Tao et al. (2007) and Song and Tao (2007) used this method to address the far-field boundary conditions associated with the wave-structure interaction in ocean engineering. Within this topic, the ability of SBFEM in modelling unbounded domain and satisfying the boundary condition at infinity is further verified. Due to the appealing features of SBFEM, it is proposed in this study to develop a SBFEM model to conduct the analysis of monopile response to the ocean wave loads.

The geometrical and mathematical formulations of the SBFEM model are provided first. The validity of the model is then examined by an equivalent FEM model using a model pile. Subsequently, the monopile structural behaviour is investigated followed by a parametric study in terms of how the wave number affects the fundamental behaviour of the monopile foundations.

PROBLEM FORMULATION

A typical geometric illustration of an offshore wind turbine with a power rating ranging from 3 MW to 6 MW is shown in Fig. 1. The rotor blades, normally with a length of 40 m-60 m, are installed on the nacelle, which contains all the important electro-mechanical components, such as the gearbox and the generator. The turbine tower, located approximately 80 m-100 m above sea level, transfers the entire load from the nacelle and the rotor blades, through the transition element, to the foundation structure.

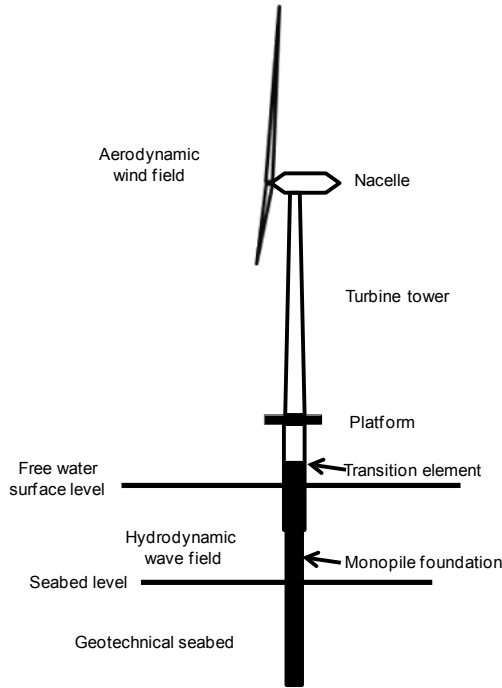


Fig. 1. Configuration of a typical monopile foundation (source: based on Leblanc (2010))

The platform (serving as the connection of the turbine tower and the transition element), the level of which, is a key parameter in the preliminary design of a wind turbine. It is located at a height of approximately 20 m above sea level. The single, freestanding monopile foundation is used to transfer the load from the tower to the seabed. It

normally has the penetration depth up to 50 m into the seabed, and is subjected to the ocean wave loads within a depth of 20 m-50 m. The entire monopile-supported wind turbine is associated with three physical aspects, separated spatially by the medium surrounding it. They can be described separately as aerodynamically associated with air above sea level, hydrodynamically associated with water between sea level and seabed level, and geotechnically associated with soil below seabed level. The main concern of this study focuses on the wave loads and the resulting structural response of the monopile foundation. The monopile is assumed to be fixed at seabed level and the external forces associated with winds and structures are not taken into consideration.

The geometric formulation, illustrating a monopile foundation subjected to wave loads in Cartesian coordinate system, is shown in Fig. 2(a), with a denoting the monopile radius, h the monopile height, d the water depth, A the wave amplitude, θ the azimuth angle along the monopile circumference measured in an anticlockwise direction and α the incident wave angle in a clockwise direction. $L-L'$, $R-R'$ are two representative lines along the monopile height respectively corresponding to $\theta = 0^\circ$ and $\theta = 180^\circ$, and will be examined in the following analysis. Ω_1 represents half of the circumferential face of the monopile foundation subjected to wave loads, with Ω_2 being its symmetric counterpart. Γ_1 represents the top and the circumferential faces of the monopile; Γ_2 refers to the monopile bottom face.

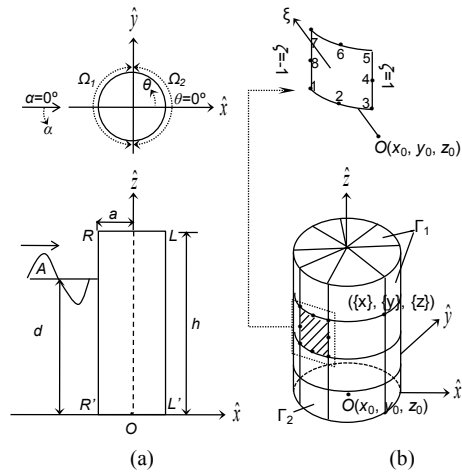


Fig. 2. Geometric illustration of the monopile foundation (a) sketch in Cartesian coordinate system; (b) SBFEM model and scaled boundary element

Based on the above geometric formulation, the equilibrium equation with respect to the stress state of the monopile foundation in the Cartesian coordinate system $(\hat{x}, \hat{y}, \hat{z})$ is shown in the vector form as:

$$[L]^T \{\sigma\} = 0 \quad (1)$$

with $[L]$ representing the differential operator. $\{\sigma\}$ is related to the strain amplitude $\{\varepsilon\}$ and the material matrix $[D]$ as:

$$\{\sigma\} = [D]\{\varepsilon\} \quad (2)$$

The strain amplitude $\{\varepsilon\}$ and displacement amplitude $\{u\}$ are related by $[L]$ in the form of:

$$\{\varepsilon\} = [L]\{u\} \quad (3)$$

Eqs. (1)-(3) govern the structural behaviour of the monopile foundation, and are to be solved with the boundary conditions specified at Γ_1 and Γ_2 .

Brief introduction of SBFEM

The original proposal of SBFEM aims at overcoming the issues encountered when solving problems involving the unbounded calculation domain using either FEM or BEM, or other numerical algorithms. These issues can be generally classified into two categories in terms of computational feasibility and performance accuracy. Instead of preceding the solution procedure with a pre-known fundamental function as is the case in BEM, which is not always accessible and depends closely on the physical nature of the problem, SBFEM explores the analytical property of the solution by solving matrix-form ordinary differential equations (ODEs). These ODEs are expressed in a new local coordinate system, termed as the scaled boundary coordinate system (ξ, η, ζ) , and are derived directly from the partial differential equations (PDEs) governing the physical problem. Therefore, a transformation from the conventional coordinate system, where the problem is originally defined, such as the Cartesian coordinate system $(\hat{x}, \hat{y}, \hat{z})$, to the scaled boundary coordinate system (ξ, η, ζ) , is performed. The benefit of this transformation is that it geometrically simplifies the representation of the computational domain, bounded or unbounded, by specifying the radial coordinate ξ ranging in $[0, 1]$ or $[1, \infty)$, which actually corresponds to describing the domain by scaling of a certain boundary. Therefore, only the boundary needs to be discretised since, through the scaling process, the discretisation of the domain can be reflected by that on the boundary. This, substantially, avoids the huge computational expense due to vast domain discretisation in FEM, especially for three-dimensional problems. The main advantages of SBFEM over FEM and BEM are tabulated in Table 1 below.

Table 1. Main features comparison amongst FEM, BEM and SBFEM

Features	Methods	FEM	BEM	SBFEM
Reduction of the spatial dimension by one, reducing data preparation and computational efforts			×	×
Analytical solution achieved inside the domain				×
No fundamental solution required		×		×
Radiation condition at infinity satisfied exactly for unbounded domain			×	×

(source: based on Song and Wolf (1997))

Avoiding the disadvantages in FEM and BEM, and at the same time combining the advantages of the two sophisticated numerical methods, SBFEM adopts the numerical concept from FEM in the discretisation and interpolation processes. As shown in Fig. 3, the element coefficient matrices from the boundary discretisation are assembled in the same way as in FEM to obtain the global coefficient matrices for the ODEs. Once the ODEs are solved analytically for the nodal function, i.e., the representation of the property variation in the radial direction, the solution of the whole domain will be sought by interpolation.

SBFEM model formulation of monopile foundation

The scaled boundary coordinate system (ξ, η, ζ) for the monopile foundation is shown in Fig. 2(b). The scaling center $O(x_0, y_0, z_0)$ is selected to coincide with the origin of the Cartesian coordinate system. The radial coordinate ξ starts as 0 from O going towards face Γ_1 of the monopile, and is defined as 1 on Γ_1 . The other two coordinates η and ζ ,

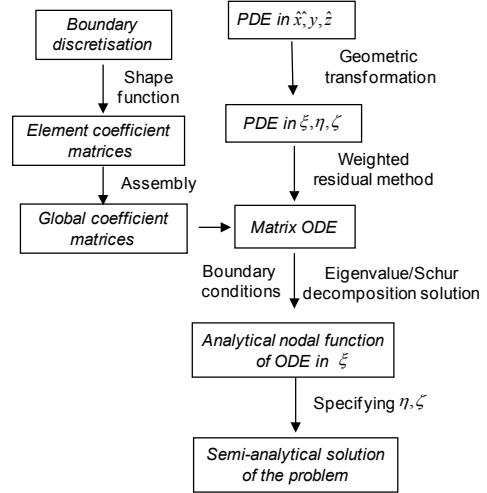


Fig. 3. SBFEM solution procedure

with magnitudes ranging from -1 to 1, locally represent the scaled boundary element mesh on face Γ_1 . No discretisation is needed for Γ_2 . The boundary condition on Γ_2 can be satisfied by applying it on to the nodes on the circumference of the monopile at the bottom level. By introducing this coordinate system, any point within the monopile in $(\hat{x}, \hat{y}, \hat{z})$ can be located by specifying ξ, η and ζ using the following transformations and the mapping functions $[N(\eta, \zeta)]$.

$$\begin{aligned}\hat{x}(\xi, \eta, \zeta) &= \xi [N(\eta, \zeta)] \{x\} + x_0 \\ \hat{y}(\xi, \eta, \zeta) &= \xi [N(\eta, \zeta)] \{y\} + y_0 \\ \hat{z}(\xi, \eta, \zeta) &= \xi [N(\eta, \zeta)] \{z\} + z_0\end{aligned}\quad (4)$$

where $\{x\}$, $\{y\}$ and $\{z\}$ are the coordinates of the discretised nodes on face Γ_1 . With this geometric mapping, the differential operator $[L]$ is reformulated using ξ, η and ζ as:

$$[L] = [b^1(\eta, \zeta)] \frac{\partial}{\partial \xi} + \frac{1}{\xi} \left([b^2(\eta, \zeta)] \frac{\partial}{\partial \eta} + [b^3(\eta, \zeta)] \frac{\partial}{\partial \zeta} \right) \quad (5)$$

with $[b^1(\eta, \zeta)]$, $[b^2(\eta, \zeta)]$ and $[b^3(\eta, \zeta)]$ being determined by the scaled boundary discretisation of face Γ_1 .

Using the same shape functions $[N(\eta, \zeta)]$ as for the boundary discretisation, the displacement amplitude is expressed as:

$$\{u(\xi, \eta, \zeta)\} = [N(\eta, \zeta)] \{u(\xi)\} \quad (6)$$

whereby $\{u(\xi)\}$ represents the nodal displacement function in the radial coordinate ξ . This function is the basic unknown function in the upcoming scaled boundary finite element equation. Once it has been solved, the displacement field within the monopile foundation can be obtained using Eq. (6) with the specified scaled boundary coordinates ξ, η and ζ , and subsequently the stress and strain fields can be calculated as:

$$\begin{aligned}\{\varepsilon\} &= \{\varepsilon(\xi, \eta, \zeta)\} = [B^1] \{u(\xi)\}_{,\xi} + \frac{1}{\xi} [B^2] \{u(\xi)\} \\ \{\sigma\} &= \{\sigma(\xi, \eta, \zeta)\} = [D] \left([B^1] \{u(\xi)\}_{,\xi} + \frac{1}{\xi} [B^2] \{u(\xi)\} \right)\end{aligned}$$

in which $[B^1]$ and $[B^2]$ are formulated as :

$$\begin{aligned}[B^1(\eta, \zeta)] &= [b^1(\eta, \zeta)] [N(\eta, \zeta)] \\ [B^2(\eta, \zeta)] &= [b^2(\eta, \zeta)] [N(\eta, \zeta)]_{,\eta} + [b^3(\eta, \zeta)] [N(\eta, \zeta)]_{,\zeta}\end{aligned}$$

Applying the weighted residual technique and Green's theorem, and through a series of manipulations, the governing PDEs. (1)~(3) are transformed into the second-order matrix-form Euler-Cauchy ODEs with respect to the nodal displacement function $\{u(\xi)\}$:

$$\begin{aligned} [E^0]\xi^2\{u(\xi)\}_{,\xi\xi} + (2[E^0] + [E^1]^T - [E^1])\xi\{u(\xi)\}_{,\xi} \\ + ([E^1]^T - [E^2])\{u(\xi)\} = 0 \end{aligned} \quad (7)$$

Eq. (7) is termed as the scaled boundary finite element equation. It is worth mentioning that in Eq. (7), only the radial coordinate ξ appears, which indicates that this equation describes the displacement variation in the radial direction. The other two coordinates η and ζ are incorporated in the coefficient matrices in the form of:

$$\begin{aligned} [E^0] &= \int_{-1}^1 \int_{-1}^1 [B^1(\eta, \zeta)]^T [D] [B^1(\eta, \zeta)] |J(\eta, \zeta)| d\eta d\zeta \\ [E^1] &= \int_{-1}^1 \int_{-1}^1 [B^2(\eta, \zeta)]^T [D] [B^2(\eta, \zeta)] |J(\eta, \zeta)| d\eta d\zeta \\ [E^2] &= \int_{-1}^1 \int_{-1}^1 [B^2(\eta, \zeta)]^T [D] [B^2(\eta, \zeta)] |J(\eta, \zeta)| d\eta d\zeta \end{aligned} \quad (8)$$

The three matrices $[E^0]$, $[E^1]$ and $[E^2]$ in Eq. (8) are first formulated for each individual element discretised on face Γ_1 and then assembled in the same way as in FEM.

The Schur decomposition has been proven to be a qualified and efficient method to solve the nodal displacement function $\{u(\xi)\}$ from Eq. (7). Following the solution procedure presented in Song (2004) and Li et al. (2010), the nodal displacement function $\{u(\xi)\}$ is expressed as:

$$\{u(\xi)\} = \xi^{-0.5} \left([\Psi_{u1}] \xi^{-[S_1]} \{C_1\} + [\Psi_{u2}] \xi^{-[S_2]} \{C_2\} \right) \quad (9)$$

with $[\Psi_{u1}]$, $[\Psi_{u2}]$ and $[S_n]$ being determined from the Schur decomposition of a matrix $[Z]$, which is formulated by the coefficient matrices of Eq. (7) as:

$$[Z] = \begin{bmatrix} [E^0]^{-1} [E^1]^T - 0.5[I] & -[E^0]^{-1} \\ -[E^2] + [E^1][E^0]^{-1} [E^1]^T & -[E^1][E^0]^{-1} + 0.5[I] \end{bmatrix}$$

where $[I]$ is the identity matrix. $\{C_1\}$ and $\{C_2\}$ in Eq. (9) are two sets of constants to be determined according to the displacement and stress boundary conditions on monopile boundaries Γ_1 and Γ_2 .

After $\{u(\xi)\}$ is derived analytically from Eq. (7), numerical interpolation is employed using Eq. (6) to determine the displacement distribution within the monopile and accordingly the stress and strain.

The proposed SBFEM model examines the structural behaviour of the monopile foundation by solving ODEs instead of PDEs as a result of coordinate transformation and boundary discretisation. It exhibits analytical features in the radial direction when solving the SBFEM equation and numerical features in the other two directions in the discretisation and interpolation processes. Only those degrees of freedom associated with the discretisation of face Γ_1 need to be solved, which significantly reduces the computational effort. The efficiency and performance of the model will be discussed in the following section.

MODEL VERIFICATION

A model pile with 1 m radius and 10 m length is used for model verification. It is subjected to a uniformly distributed pressure acting normally to its circumferential face with a magnitude of 3×10^8 Pa. The proposed SBFEM model is employed to investigate the model pile's displacement. Linear elastic material properties with Young's modulus E of 2.8×10^{10} Pa and Poisson's ratio ν of 0.25 are assigned to the model pile. The scaling centre in SBFEM model is chosen at the centre of the model pile. From convergence test, all the faces of the pile are

discretised into 224 quadratic eight-node quadrilateral isoparametric elements. The shape functions and the node numbering scheme are shown in Eq. (10) and Fig. 2(b), respectively.

$$\begin{aligned} N_1(\eta, \zeta) &= \frac{1}{4}(1-\eta)(\zeta-1)(\eta+\zeta+1) & N_2(\eta, \zeta) &= \frac{1}{2}(\eta^2-1)(\zeta-1) \\ N_3(\eta, \zeta) &= \frac{1}{4}(\zeta-1)(1+\eta)(1-\eta+\zeta) & N_4(\eta, \zeta) &= \frac{1}{2}(\eta+1)(1-\zeta^2) \\ N_5(\eta, \zeta) &= \frac{1}{4}(\eta+1)(\zeta+1)(\eta+\zeta-1) & N_6(\eta, \zeta) &= \frac{1}{2}(1-\eta^2)(\zeta+1) \\ N_7(\eta, \zeta) &= \frac{1}{4}(\eta-1)(\zeta+1)(\eta-\zeta+1) & N_8(\eta, \zeta) &= \frac{1}{2}(\eta-1)(\zeta^2-1) \end{aligned} \quad (10)$$

The displacement at the top of the model pile in the x direction converges to 8.04 mm, and in the z direction is 52.07 mm.

A comparative FEM analysis, using the ANSYS package is also carried out for the same case. Three dimensional 20-node hexahedral solid elements are used in the FEM discretisation. A convergence test reveals that 28 elements are needed in the circumferential direction, 5 in the radial direction and 50 along the height. The pile head displacements in the x and z directions reach 8.04 mm and 52.35 mm, respectively.

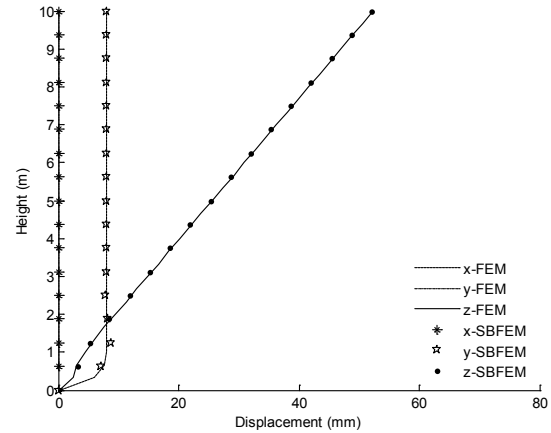


Fig. 4. Displacements comparison from SBFEM and FEM models

The displacements from both the proposed SBFEM model and the FEM model are plotted against the height of the pile in Fig. 4(c). The comparison shows the appealing feature of the proposed SBFEM model in analysing the pile's behaviour using fewer elements, which guarantees the favourability of the model for future analysis.

WAVE PRESSURE FORMULATION

The hydrostatic pressure p_h , varying with the vertical distance z measured along the monopile height under the free water surface level, follows the formation presented below:

$$p_h = \rho_w g z \quad (11)$$

with ρ_w representing the water density and g the gravitational acceleration.

In real ocean environments, short-crested waves are very likely to be generated and therefore, are the most common form of waves when winds blowing over the surface of the ocean. Since Jeffreys (1924) developed the theory of the short-crested waves in 1924, many researchers have investigated its kinematic and dynamic properties, and also the diffraction, reflection and radiation phenomena due to its

interactions with coastal and offshore structures. Zhu (1993) studied systematically the loads exerted by short-crested waves on a cylindrical pile of coastal or offshore structures, and presented an analytical expression. The magnitude of the wave pressure is shown as:

$$p_m(a, \theta, z) = \frac{\rho_w g A \cosh k(z+d)}{2 \cosh kd} \sum_{m=0}^{\infty} \sum_{n=0}^{\infty} \varepsilon_m \varepsilon_n i^m Q_{mn}(a, \theta) \quad (12)$$

It can be seen that the wave pressure exerted on the cylindrical pile spatially is a function of the azimuth angle θ along the circumference of the pile, and z is also related to the radius a of the pile, and the properties of the short-crested waves, i.e., the wave amplitude A and the wave number k . d is the water depth. ε_m , ε_n and $Q_{mn}(a, \theta)$ are related to the series terms and are defined as:

$$\varepsilon_m, \varepsilon_n = \begin{cases} 1 & m, n = 0 \\ 2 & m, n \neq 0 \end{cases}$$

$$Q_{mn}(a, \theta) = [J_m(k_x a) J_{2n}(k_y a) - A_{mn} H_{m+2n}(ka)] \cos(m+2n)\theta$$

$$+ [J_m(k_x a) J_{2n}(k_y a) - B_{mn} H_{|m-2n|}(ka)] \cos(m-2n)\theta \quad (13)$$

where

$$A_{mn} = \frac{k_x J'_m(k_x a) J_{2n}(k_y a) + k_y J_m(k_x a) J'_{2n}(k_y a)}{k H'_{m+2n}(ka)} \quad (14)$$

$$B_{mn} = \frac{k_x J'_m(k_x a) J_{2n}(k_y a) + k_y J_m(k_x a) J'_{2n}(k_y a)}{k H'_{|m-2n|}(ka)} \quad (15)$$

In Eqs. (13)~(15), J represents the Bessel function of the first kind and H represents the Hankel function. k_x and k_y explain the periodic property of the short-crested waves at the free-surface level in the x and y directions, respectively. They are related to the incident wave angle α as:

$$k_x = k \cos \alpha, \quad k_y = k \sin \alpha \quad (16)$$

Normally, the wave period T for wind waves in ocean environment ranges from 1 second to 25 seconds. With this condition, wave number k in Eq. (12) can be evaluated iteratively from the wave dispersion equation, $(2\pi/T)^2 = gk \tanh(kd)$, given water depth d . An illustration of the short-crested wave pressure exerted on a 2.5 m radius monopile foundation with $A=1$ m, $k=0.1$, $\alpha=0^\circ$ in a 30 m depth water condition is shown in Fig. 5. The pressure is plotted against the azimuth angle θ around the circumference of the monopile. The pressure is found to be symmetrically distributed around the monopile circumference with respect to the x axis. Therefore, only the part from $\theta=0^\circ$ to $\theta=180^\circ$ is shown. The total wave pressure acting on a monopile foundation results from the superimposition of the hydrostatic pressure and the dynamic wave pressure. Since the hydrostatic part is zero at the free surface level, the total wave pressure coincides with the dynamic wave pressure as shown in Fig. 5.

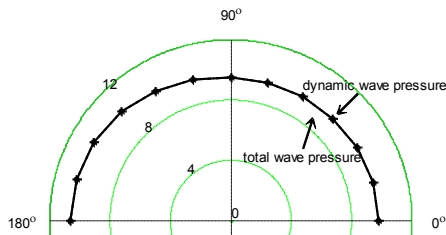


Fig. 5. Wave pressure along monopile circumference at free surface level (unit: MPa)

The dynamic pressure predominates at the free surface level where $z=30$ m, and diminishes rapidly with the increase of depth. At the same time, the hydrostatic component grows and takes the most significant part.

STRUCTURAL RESPONSE OF MONOPILE FOUNDATION

With the proposed SBFEM model, the structural response of a monopile foundation is studied with the total wave pressure presented in the above section. The geometric dimensions for the monopile foundation and the wave parameters are listed in Table 2. Using the same quadratic eight-node quadrilateral isoparametric elements as for the model pile, all the faces of the monopile are discretised into 408 elements.

Table 2. Physical parameters for monopile foundations and wave loads

Physical quantities	Representative symbols	Magnitudes
Monopile radius (m)	a	2.5
Monopile height (m)	h	40
Young's modulus (Pa)	E	2.8×10^{10}
Poisson's ratio	γ	0.25
Water depth (m)	d	30
Wave amplitude (m)	A	1
Incident wave angle ($^\circ$)	α	0
Total wave number	k	0.10

The total x , y and z displacement components along $L-L'$, corresponding to $\theta=0^\circ$, of the monopile are shown in Fig. 6. With $k=0.10$, $A=1$ m, $\alpha=0^\circ$ and $d=30$ m, the maximum x displacement examined at the monopile head level is 0.29 mm, with the z component displacement being 0.05 mm. Symmetry of the pressure distribution with respect to the incident wave direction results in zero displacement in the y direction. The negative displacements at the bottom of the monopile, with the maximum absolute values being 0.01 mm in the x direction, is caused by the dominant hydrostatic pressure acting at the seabed level where $z=0$ m.

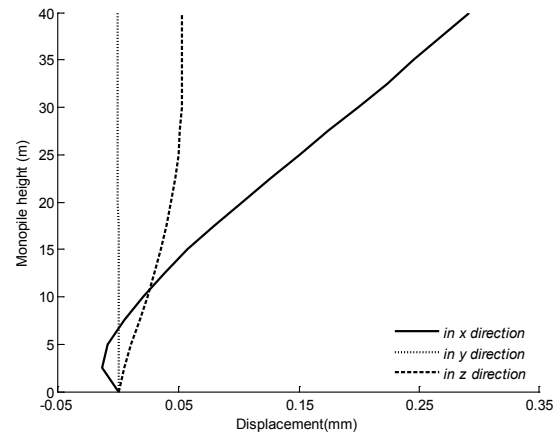


Fig. 6. Total x , y and z components of monopile displacement along $L-L'$ at $A=1$ m, $\alpha=0^\circ$ and $k=0.10$

The displacement components at the monopile head level are plotted in the polar coordinate system in Fig. 7 to illustrate the displacement variation in the circumferential direction. Being the maximum

displacement at the monopile head level, the x component is equally distributed around the monopile circumference, with a magnitude of 0.29 mm. The y component displacement is zero due to the symmetry with respect to the x axis of the problem. The z component, however, shows a minimum of 0.05 mm at $\theta=0^\circ$ and a maximum of 0.10 mm at $\theta=180^\circ$.

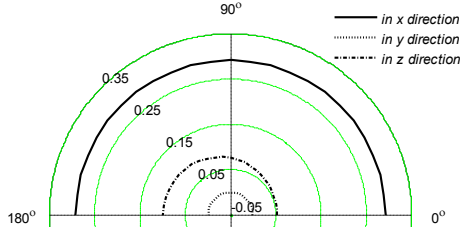


Fig. 7. Total x , y and z displacements along circumference at the monopile head level at $A=1\text{m}$, $\alpha=0^\circ$ and $k=0.10$ (unit: mm)

To understand how each part, i.e., the dynamic wave pressure and the hydrostatic pressure, contributes to the monopile behaviour under the total wave loads, the displacement components in the x and z directions of the monopile foundation under pure dynamic wave pressure and pure hydrostatic pressure are shown individually. As the symmetry of the problem results in zero displacement in the y direction, only x and z components of the monopile displacement are examined. A greater reading in the x displacement component at the monopile head level from the dynamic part, the magnitude of which being 0.29 mm, than that from the hydrostatic part, which is zero, is displayed in Fig. 8(a). On the contrary, the z displacement from the hydrostatic pressure, uniformly distributed around the circumference at the monopile head level with a magnitude of 0.07 mm, exceeds that from the pure dynamic wave pressure by a minimum of 0.05 mm, which is examined at $\theta=180^\circ$, as shown in Fig. 8(b).

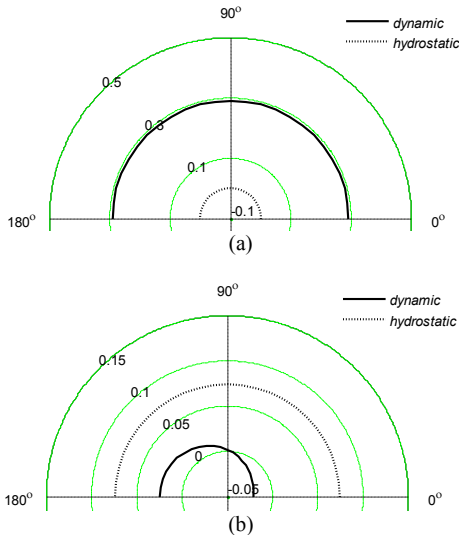


Fig. 8. Displacement along circumference at the monopile head level from dynamic wave pressure and hydrostatic pressure respectively (a) x component displacement; (b) z component displacement (unit: mm)

Furthermore, Fig. 8(b) illustrates that the difference in z component displacement at $\theta=0^\circ$ and $\theta=180^\circ$ shown in Fig. 7 can be attributed to

the dynamic wave pressure. Predominant at the free surface level, the dynamic wave pressure is relatively greater on the upstream face, corresponding to Ω_1 in Fig. 2, than that on Ω_2 , as shown in Fig. 5. This pressure difference makes the monopile bend towards positive x direction, which induces a negative z displacement along $L-L'$ (shown in Fig. 9(b)) at $\theta=0^\circ$, with a magnitude of -0.02 mm at the monopile head level showing the shrinkage at the Ω_2 side; and a positive z displacement along $R-R'$ at $\theta=180^\circ$, with a magnitude of 0.02 mm (read from Fig. 8(b)) at $z=40$ m demonstrating the elongation at the Ω_1 side.

Producing no pressure difference on Ω_1 and Ω_2 , the hydrostatic pressure does not contribute to the unevenness in the z component displacement at $\theta=0^\circ$ and $\theta=180^\circ$. Instead, due to its significant magnitude at a lower level compared with its dynamic counterpart, the hydrostatic pressure elongates the monopile vertically by a magnitude of 0.07 mm (read from Fig. 9(b)). Therefore, a positive z displacement at the monopile head level at $\theta=0^\circ$ with a magnitude of 0.05 mm results since, with the combined effect, the negative part from the dynamic wave pressure is cancelled out by the superimposition of the positive part from the hydrostatic pressure. It is also noted, from Fig. 9, that the x displacement from the hydrostatic part and the z displacements from both the dynamic and hydrostatic parts remain at a constant level once z is greater than 30 m, corresponding to the part of the monopile foundation which is free from the wave loads. The x displacement from the dynamic wave pressure, however, increases linearly with the monopile height above the free surface level.

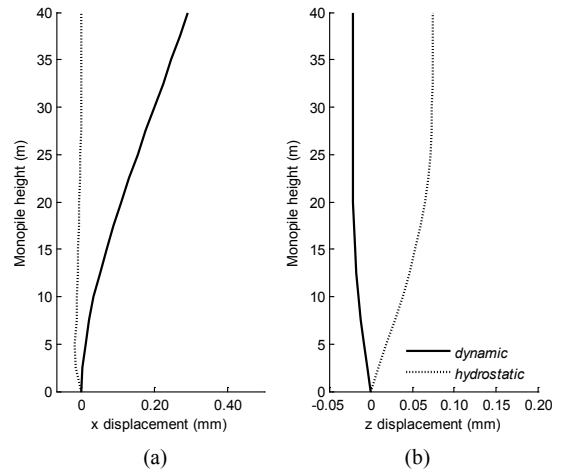


Fig. 9. Displacements along $L-L'$ of the monopile foundation from dynamic wave pressure and hydrostatic pressure respectively (a) x component displacement; (b) z component displacement

WAVE NUMBER EFFECT ON MONOPILE BEHAVIOUR

Such key parameters of the dynamic wave pressure are of great significance to the monopile behaviour as the wave numbers, the incident wave angles and the wave amplitudes. Considering the real situation where these parameters are varying within a certain range, a study on the monopile response to the variation in these parameters is carried out to gain further insight into the functional performance of the monopile foundation. In this study, the analysis mainly focuses on how the wave number affect the wave pressure and accordingly the monopile behaviour.

By specifying wave numbers k at 0.04, 0.07, 0.10, and 0.13, and keeping other parameters listed in Table 2 fixed, the wave pressure and

the monopile behaviour under different wave loading conditions are examined.

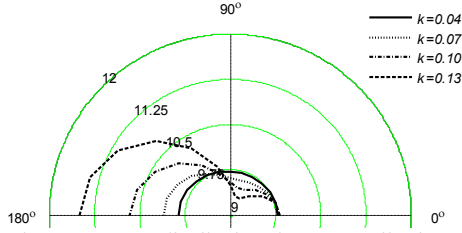


Fig. 10. Total wave pressure distribution along monopile circumference at free surface level (unit: MPa)

Fig. 10 shows the total wave pressure distribution for varying wave numbers around the monopile circumference at the free surface level. With the incident wave propagating in the positive x direction, the wave pressure generated with a relatively small wave number is distributed evenly around the monopile circumference. When the wave number k gradually increases from 0.04 to 0.13 by increments of 0.03, the wave pressure acting on Ω_1 increases substantially, whereas that on Ω_2 decreases. Consequently, this causes the increase in the magnitude of the resultant force acting on the monopile foundation. Therefore, the resultant force, acting in the positive x direction, induces maximum x direction displacements at the monopile head level of 0.03 mm, 0.13 mm, 0.29 mm and 0.50 mm for k equating to 0.04, 0.07, 0.10 and 0.13, respectively (see Fig. 11(a)). Plotting these maximum x displacements against the wave numbers k in Fig. 12(a) and examining the slope of the curve, it can be concluded that as k becomes greater, the increase of the maximum x displacement also becomes more remarkable.

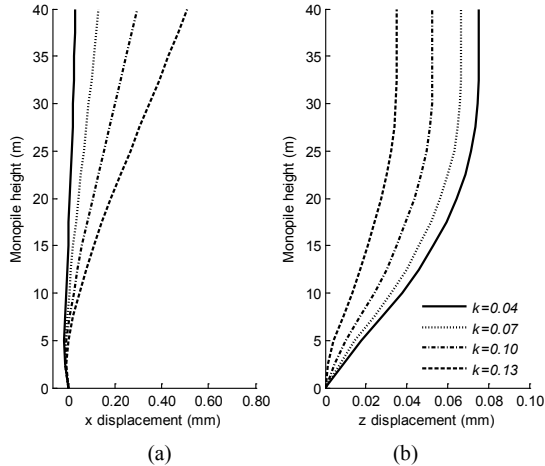


Fig. 11. Displacements along $L-L'$ of the monopile foundation (a) x component displacement; (b) z component displacement

The displacement along $L-L'$ of the monopile foundation in the z direction is shown in Fig. 11(b) for different wave numbers. Referring back to Fig. 10, it shows that the greater the wave number, the greater the resultant force acting on the monopile foundation, accordingly, the more the monopile foundation bends, the greater the magnitude of the negative z displacement along $L-L'$. When superimposed by the positive value from the hydrostatic part, the displacement resulting from a greater wave number is shown to be reduced. Therefore, the z displacement decreases from 0.08 mm, 0.07 mm, 0.05 mm to 0.04 mm when the wave number k changes from 0.04, 0.07, 0.10 to 0.13. This

can also be noticed in Fig. 12(b), which plots the maximum z component displacement, read at the monopile head level, against different wave numbers.

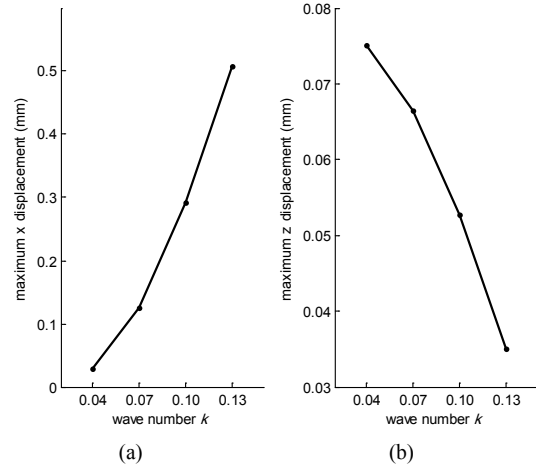


Fig. 12. Maximum displacement versus wave number (a) displacement in the x direction; (b) displacement in the z direction

The x and z direction displacements at the monopile head level are plotted in the polar coordinate system to investigate their variations with respect to the azimuth angle θ . The x displacements for different wave numbers are uniformly distributed all around the monopile circumference, whereas the difference in the z displacement at $\theta = 0^\circ$ and $\theta = 180^\circ$, seen from Fig. 13(b), becomes more significant as the wave number rises.

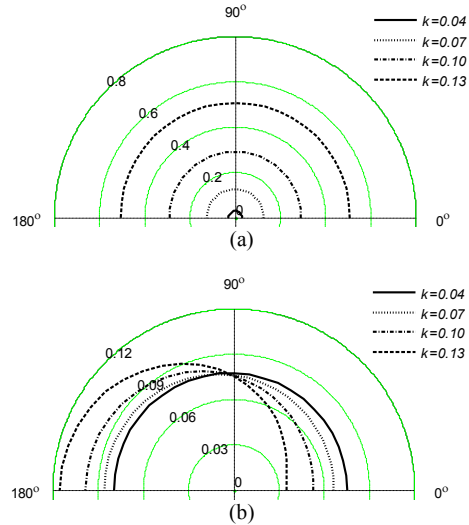


Fig. 13. Displacement around circumference at the monopile head level (a) x component displacement; (b) z component displacement (unit: mm)

CONCLUSIONS

A three-dimensional SBFEM model is proposed herein to study the structural behaviour of a monopile foundation when subjected to ocean wave loads. By introducing a local scaled boundary coordinate system,

the SBFEM model reduces the PDEs governing the structural behaviour of the monopile foundation to matrix-form ODEs in the radial direction. Only the degrees of freedom associated with the discretised monopile boundaries are involved when formulating the coefficient matrices of the ODEs, which considerably reduces the computational investment. Subsequently, the ODEs are solved analytically for the nodal displacement function, which represents the displacement variation in the radial direction. Adopting the same interpolation concept as that from FEM, SBFEM model explores the displacement field within the monopile foundation by specifying the radial coordinate in the nodal displacement function and the other two coordinates in the shape functions. This model thus demonstrates analytical as well as numerical features in the solution process, and has shown favourable applicability in modelling monopile behaviour by comparison with an equivalent FEM model.

The structural response of the monopile foundation to the wave loads is studied using the proposed SBFEM model. The contributions of the dynamic wave pressure and the hydrostatic pressure to the monopile behaviour are carefully investigated. The displacement in the x direction and the displacement difference in the z direction at $\theta = 0^\circ$ and $\theta = 180^\circ$ are mainly associated with the dynamic wave pressure. The hydrostatic pressure, uniformly distributed along the monopile circumference, provides significant positive displacement in the z direction.

The wave number effect on the monopile behaviour is examined. It is found that the displacement in the x direction increases as the wave number rises, whereas, the z displacement along $L-L'$ decreases. However, the difference in z displacement when $\theta = 0^\circ$ and $\theta = 180^\circ$ becomes more noticeable as the wave number increases.

The model presented in this study demonstrates the favourable capability of SBFEM in modelling the structural behaviour of the monopile foundation, and is expected to be applicable to other coastal and offshore structures. The results from the parametric study are suggested to provide further information when wave effect is of the greatest concern. Further analysis, in terms of how the wave amplitude and incident wave angle affect the monopile behaviour can be performed to gain further insight into the monopile behaviour under the wave loads.

REFERENCES

- Achmus, M, Kuo, YS, and Abdel-Rahman, K (2009). "Behavior of monopile foundations under cyclic lateral load," *Computers and Geotechnics*, Vol 36, No 5, pp 725-735.
- Deeks, AJ, and Cheng, L (2003). "Potential flow around obstacles using the scaled boundary finite-element method," *International Journal for Numerical Methods in Fluids*, Vol 41, No 7, pp 721-741.
- Doherty, JP, and Deeks, AJ (2003). "Scaled boundary finite-element analysis of a non-homogeneous elastic half-space," *International Journal for Numerical Methods in Engineering*, Vol 57, No 7, pp 955-973.
- Eicher, JA, Guan, H, and Jeng, DS (2003). "Stress and deformation of offshore piles under structural and wave loading," *Ocean Engineering*, Vol 30, No 3, pp 369-385.
- Jeffreys, H (1924). "On water waves near the coast," *Philosophical Magazine Series 6*, Vol 14, pp 44-48.
- Kellezi, L, and Hansen, PB (2003). "Static and dynamic analysis of an offshore mono-pile windmill foundation," *Offshore mono-pile*, Lyngby, Denmark, GEO - Danish Geotechnical Institute.
- Khani, MHBM (2007). "Dynamic soil-structure interaction analysis using the scaled boundary finite-element method," The University of New South Wales. Doctor of Philosophy. Sydney, Australia.
- Leblanc, C, Houlby, GT, and Byrne, BW (2010). "Response of stiff piles in sand to long-term cyclic lateral loading," *Geotechnique*, Vol 60, No 2, pp 79-90.
- Li, BN (2007). "Extending the scaled boundary finite element method to wave diffraction problems," The University of Western Australia. Doctor of Philosophy. Perth, Australia.
- Li, M, Song, H, Guan, H, and Zhang, H (2010). "Schur decomposition in the scaled boundary finite element method in elastostatics," 9th World Congress on Computational Mechanics and 4th Asian Pacific Congress on Computational Mechanics, Sydney, Australia.
- Mei, CC (1989). *The Applied Dynamics of Ocean Surface Waves*, Singapore, World Scientific.
- Song, CM (2004). "A matrix function solution for the scaled boundary finite-element equation in statics," *Computer Methods in Applied Mechanics and Engineering*, Vol 193, No 23-26, pp 2325-2356.
- Song, CM, and Wolf, JP (1997). "The scaled boundary finite-element method - Alias consistent infinitesimal finite-element cell method - For elastodynamics," *Computer Methods in Applied Mechanics and Engineering*, Vol 147, No 3-4, pp 329-355.
- Song, H, and Tao, LB (2007). "Short-crested wave interaction with a concentric porous cylindrical structure," *Applied Ocean Research*, Vol 29, No 4, pp 199-209.
- Tao, LB, Song, H, and Chakrabarti, S (2007). "Scaled boundary FEM solution of short-crested wave diffraction by a vertical cylinder," *Comput. Methods Appl. Mech. Engrg.*, Vol 197, pp 232-242.
- Wolf, JP (2002). "Response of unbounded soil in scaled boundary finite-element method," *Earthquake Engineering & Structural Dynamics*, Vol 31, No 1, pp 15-32.
- Wolf, JP, and Song, CM (1996). *Finite-element modelling of unbounded media*, Chichester, Wiley.
- Yang, ZJ (2006). "Fully automatic modelling of mixed-mode crack propagation using scaled boundary finite element method," *Engineering Fracture Mechanics*, Vol 73, No 12, pp 1711-1731.
- Yang, ZJ, and Deeks, AJ (2007). "Fully-automatic modelling of cohesive crack growth using a finite element-scaled boundary finite element coupled method," *Engineering Fracture Mechanics*, Vol 74, No 16, pp 2547-2573.
- Zaaijer, MB (2006). "Foundation modelling to assess dynamic behaviour of offshore wind turbines," *Applied Ocean Research*, Vol 28, pp 45-57.
- Zhu, S (1993). "Diffraction of short-crested waves around a circular cylinder," *Ocean Engineering*, Vol 20, No 4, pp 389-407.